Topological Analysis of the Electron Density Distribution of Bis(diiminosuccinonitrilo)nickel, $Ni(C_4N_4H_2)_2$: Comparison between Experiment and Theory

Tsong-Song Hwang and Yu Wang*,†

Department of Chemistry, National Taiwan University, Taipei, Taiwan, ROC

Received: July 29, 1997; In Final Form: November 10, 1997

A quantitative description of chemical bonds in bis(diiminosuccinonitrilo)nickel, $Ni(disn)_2$, is made in terms of topological properties of electron densities. These properties are obtained both from an X-ray diffraction experiment and from molecular orbital calculations. The asphericity in electron density around the Ni ion is surely observable from the Laplacian of the electron density with density accumulation in the d_π direction but density depletion along the d_σ (Ni−N) direction. On the basis of the topological properties at bond critical points, the bonding between Ni and the imino nitrogen atom is classified as mainly a closed-shell interaction but with some covalent character. The bonds within the ligand, disn, are all shared interactions, and the bond order is reflected clearly from the density at the critical point, $\rho(\mathbf{r}_c)$. The π-delocalization of the molecule is precisely indicated by the bond ellipticity and is illustrated by Fermi-hole distribution. Atom domains in the molecule are demonstrated. Molecular electrostatic potential is derived both from experiment and from MO calculations. For all the properties, the agreement between experiment and theory is reasonable.

Introduction

Charge density distribution of the title compound has been investigated recently through deformation density distribution on a combined experimental and theoretical study.[1] Topological theory of atoms in molecules[2] brings in a new insight into chemical bonding characterization. The bias[3−6] on how to deal with the proper model for the promolecule is no longer a worry since the topological analysis is based entirely on the total electron density of the molecule. This analysis has been mainly applied on the basis of molecular orbital calculations.[7−9] Recently, a few examples were given using experimental electron density.[10−14] Such application to experimental X-ray diffraction data requires the multipole model of atomic density.[15−17] The results of the topological analysis do provide precise information on chemical bonding which, in fact, enhances the value of such a multipole model. Since the bond topological properties give a quantitative characterization of chemical bonds, it is important to compare the properties derived both from experiment and from wave functions. Recently, the classification of chemical bonds based on topological analysis of electron localization functions (ELF)[18,19] demonstrated even clearer features concerning lone pairs and single, double, or triple bonds. The result of such ELF analysis correlates precisely with VSEPR theory. The purpose of this work is to obtain a quantitative characterization of chemical bonds through topological analysis in a combined experimental and theoretical study. The magnitude of the electron density at the bond critical point, $\rho(\mathbf{r}_c)$, correlates directly with the bond distance and the bond order. The Laplacian of electron density depicts the charge concentration and depletion. This topology of Laplacian of electron density also provides the physical basis for the Lewis and VSEPR models.[2,20−22] When $\nabla^2\rho(\mathbf{r}) < 0$, it means the electron density is locally concentrated at $\mathbf{r}$, and when $\nabla^2\rho(\mathbf{r}) > 0$, the electron density is locally depleted at $\mathbf{r}$. In addition, the Laplacian value at a (3, −1) bond critical point provides the description of the interaction between the bonded atoms as being closed shell (ionic) or electron shared (covalent).[2] The bond ellipticity, ϵ, is a direct indicator of the π bond character. The Fermi-hole function[23−25] is a measure of Pauli repulsion and is very useful for realizing the bond delocalization. Molecular electrostatic potential[26] (MEP) is helpful for predicting a long-range electrostatic interaction[27−33] such as protonation and intramolecular hydrogen bonds.

Computation Details

The total electron density of the molecule from experiment is calculated on the basis of the multipole parameters which are given in our previous work[1]. Although the exact molecular symmetry in the crystal is C_i, the actual geometry can be considered as D_{2h} within three standard deviations. The multipole coefficients, P_{lm}, were constrained in D_{2h} fashion.[1] Since we are mainly interested in the molecular properties, total electron density is only calculated for a single molecule both in experiment and in theory. The total electron density from theory is obtained by an ab initio molecular orbital calculation at HF level, which takes no account of electron correlation effects. The basis set of Ni atom is [14, 9, 5]/[6, 3, 2].[34] Basis sets of C, N, and H atoms are taken from 6-31G**. The geometry of the molecule is taken to be D_2h by imposing a C_2 symmetry on the coordinates obtained from X-ray diffraction data.[1]

A critical point (CP), $\mathbf{r}_c$, is a point satisfying the condition $\nabla\rho(\mathbf{r}_c) = 0$, where

$$\nabla\rho(\mathbf{r}) = i\frac{\partial\rho(r)}{\partial x} + j\frac{\partial\rho(r)}{\partial y} + k\frac{\partial\rho(r)}{\partial z}$$

This is made by the Newton−Raphson method, and the initial position can be assigned at a point near the expected CP. The gradient vector field of charge density is represented through a display of the trajectories traced out by the vector $\nabla\rho$. A

* To whom correspondence should be addressed.
† E-mail: yuwang@chem38.ch.ntu.edu.tw.

S1089-5639(97)02468-7 CCC: $15.00
Published on Web 04/30/1998

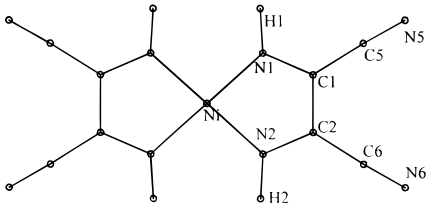

Figure 1. Molecular geometry and the atomic labeling of the molecule.

trajectory of $\nabla\rho$ (gradient path) starts from some arbitrary point $\mathbf{r}_0$ and moves with a step size of Δr in the direction of $\nabla\rho(\mathbf{r}_0)$ and then repeats with the same procedure at the next step until such path terminates. The gradient vector field map in this work is drawn in such a way that 48 equally spaced directions are started around each nucleus on the projected molecular plane. Bond paths are pairs of gradient vectors originated from bond critical point (BCP) and terminated at neighboring atomic nucleus, in other words, the path which goes through the maximum local density. An atom domain is a surface of zero flux which normally pass through BCPs and is perpendicular to bond paths; therefore, the atom domain characterizes a unique volume around each nucleus. MEP is obtained according to[26]

$$V(\mathbf{r}) = \sum_{\alpha}^{\text{nuclei}} \frac{Z_\alpha}{|r_\alpha - r|} - \int \frac{\mathrm{d}r_1\, \rho(r_1)}{|r_1 - r|}$$

where Z_α and r_α are the charge and the location of nucleus α, respectively.

The Gaussian94 program[35] is used to do the MO calculations. The Fermi-hole function is calculated from HF calculation and displayed as a contour map to illustrate the electron delocalization. Molecular total electron density, BCP, bond path, atom domain, Laplacian, field gradient vector, and MEP are calculated using the PROP[36] and AIMPAC[37] programs respectively for experiment and theory.

Results and Discussion

Topological Properties and Critical Points. The molecular structure based on the diffraction data[1] is given in Figure 1. A local maximum in electron density corresponding to a (3, −3) CP is found at each atomic site in the molecule. A (3, −1) BCP is located at each chemical bond in the molecule. An additional (3, 1) ring critical point is found at the center of the five-membered ring both from experiment and from calculation.

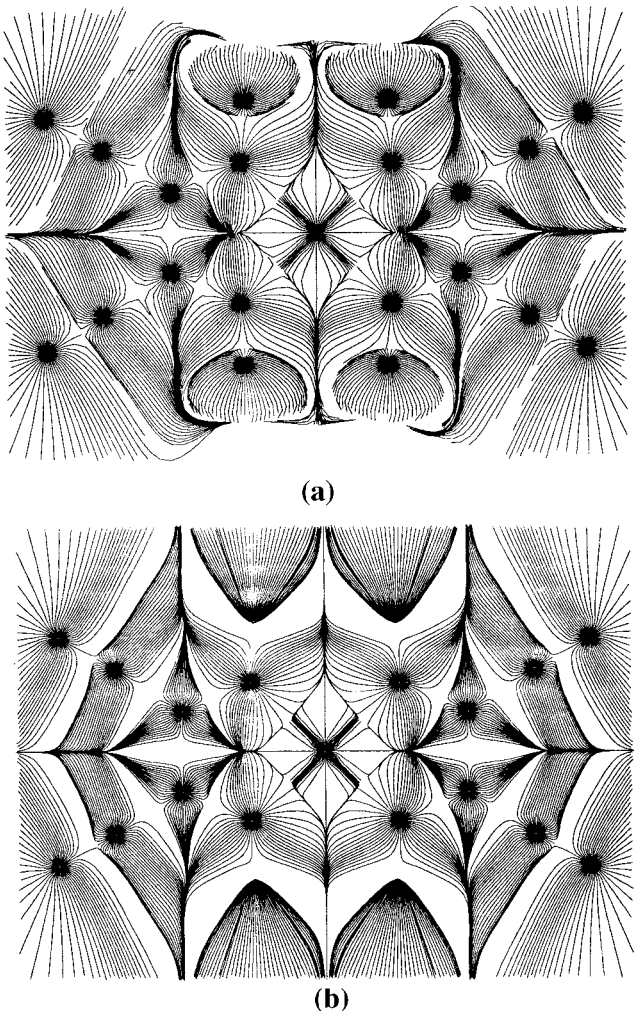

Figure 2. Gradient vector field from (a) experiment and (b) calculation.

Starting from the BCP, there is only one direction to go, uphill in the density, and such a path along the direction of the steepest ascent will always terminate at a (3, −3) CP, the nucleus. Such a trajectory is a topological bond path. The bond paths from experiment and from theory coincide well with the actual molecular structure. The only significant difference between experiment and theory is in the region very close to the Ni nucleus, where the bond path angle of N−Ni−N is slightly smaller as calculated than as found experimentally (black lines

TABLE 1: Properties Associated with Bond Critical Points (1st Line Experimental Values; 2nd Line Theoretical Values)

bond (BL (Å))[a]	d_1[b] (Å)	d_2[c] (Å)	Hessian eigenvalue[d] (e Å^{-5}) λ_1	λ_2	λ_3	$\nabla^2\rho(\mathbf{r}_c)$[e] (e Å^{-5})	ϵ $(\lvert\lambda_1/\lambda_2\rvert - 1)$	$\lvert\lambda_1/\lambda_3\rvert$	$\rho(\mathbf{r}_c)$ (e Å^{-3})
Ni−N1	0.91	0.92	−5.49	−5.17	22.94	12.28	0.06	0.24	0.94
(1.828)	0.86	0.97	−3.11	−2.74	26.27	20.41	0.14	0.12	0.78
N1−C1	0.81	0.52	−20.97	−16.67	16.98	−20.65	0.26	1.23	2.31
(1.332)	0.88	0.44	−20.51	−16.42	15.54	−21.39	0.25	1.32	2.39
C1−C2	0.70	0.72	−16.82	−13.77	12.72	−17.87	0.22	1.32	2.05
(1.411)	0.70	0.70	−17.55	−13.83	7.01	−24.36	0.27	2.50	2.18
C1−C5	0.72	0.71	−14.54	−12.98	13.68	−13.84	0.12	1.06	1.90
(1.432)	0.65	0.78	−14.87	−13.74	5.55	−23.06	0.08	2.68	1.99
C5−N5	0.46	0.70	−27.03	−25.73	30.41	−22.35	0.05	0.89	3.27
(1.152)	0.39	0.76	−24.53	−23.81	65.10	16.76	0.03	0.38	3.25
N1−H1	0.79	0.29	−20.21	−19.39	31.01	−8.59	0.04	0.65	1.64
(1.08)	0.81	0.27	−23.57	−23.16	14.55	−32.19	0.02	1.62	1.91
RCP[f]			−0.67	1.30	3.32	3.95			0.26
			−0.64	1.82	4.17	5.35			0.22

[a] BL is the bond length from experiment constrained in D_{2h}. [b] d_1 is the distance between BCP to the first atom in the bond. [c] d_2 is the distance between BCP to the second atom in the bond. [d] λ_1, λ_2, and λ_3 are Hessian eigenvalues at the critical point. λ_3 is along the bond path, and λ_1 and λ_2 are along the directions perpendicular to the bond path. [e] $\nabla^2\rho(\mathbf{r}_c) = \lambda_1 + \lambda_2 + \lambda_3$, Laplacian value at CP. [f] RCP is the ring critical point.

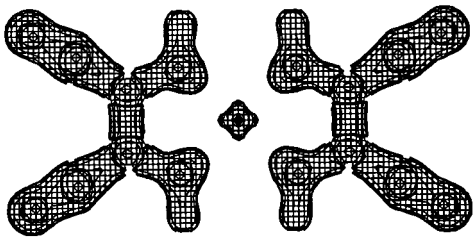

Figure 3. Isovalue surface of the zero Laplacian from the MO calculations.

in Figure 5a, b). This difference is even clearly displayed in the gradient vector maps shown in Figure 2. The relative distribution of the tightness and looseness of the gradient paths around Ni is quite different near the Ni nucleus (Figure 2a,b). Detailed properties at BCP are listed in Table 1. In general, the values from experiment and theory are in reasonably good agreement with each other. However, significant discrepancies are found in the $\nabla^2\rho(\mathbf{r}_c)$ values of the short triple C5−N5 and N−H bonds. This is due to the fact that the BCP are apparently very close to the electropositive centers C (0.39 Å) and H (0.29 Å). This will lead to the transfer of charge from the C or H to N, as indicated by Bader for C−O and C−S bonds.[2] Such polarization may yield the fact that the BCP lies just within the inner shell of charge depletion of C or H nucleus and thus gives a large positive λ_3 value. This is the case for C5−N5 triple bond, and the theoretical value of λ_3 is much larger than that of experimental one, so that the sign of the $\nabla^2\rho(\mathbf{r}_c)$ value, i.e., $\lambda_1 + \lambda_2 + \lambda_3$, is different between experiment and theory. Nevertheless, simply looking at λ_1 and λ_2 values, they are all large negative numbers indicating there is electron concentration along the bond. The different positions for the BCPs between experiment and theory are also shown in Table 1. In general, the difference in d_1 and d_2 is larger from MO calculation than that from experiment, especially for the bond with polar electron density distribution. The strong effect of such difference on the λ_3 value is quite pronounced. From the table, it is apparent that all bonds in the ligand are shared interactions. However the bond between Ni and nitrogen atom is more like a closed shell interaction with λ_1/λ_3 much less than 1, a positive $\nabla^2\rho(\mathbf{r}_c)$ value, and a small value of $\rho(\mathbf{r}_c)$. This is quite consistent with our earlier NBO analysis,[1] defining it as mainly a "dative" or "coordinated" bond with a small percentage of covalent character. A recent work[14] points out that a positive Laplacian value at BCP does not necessarily indicate a closed-shell, noncovalent interaction, especially when the charge distribution is diffuse. The $\rho(\mathbf{r}_c)$ value is often recognized as a number highly correlated with the bond order. Sure enough, the C5−N5 triple bond has the highest $\rho(\mathbf{r}_c)$ value of 3.27. The delocalized C−C, C−N bonds have the values of 2.0−2.4. The

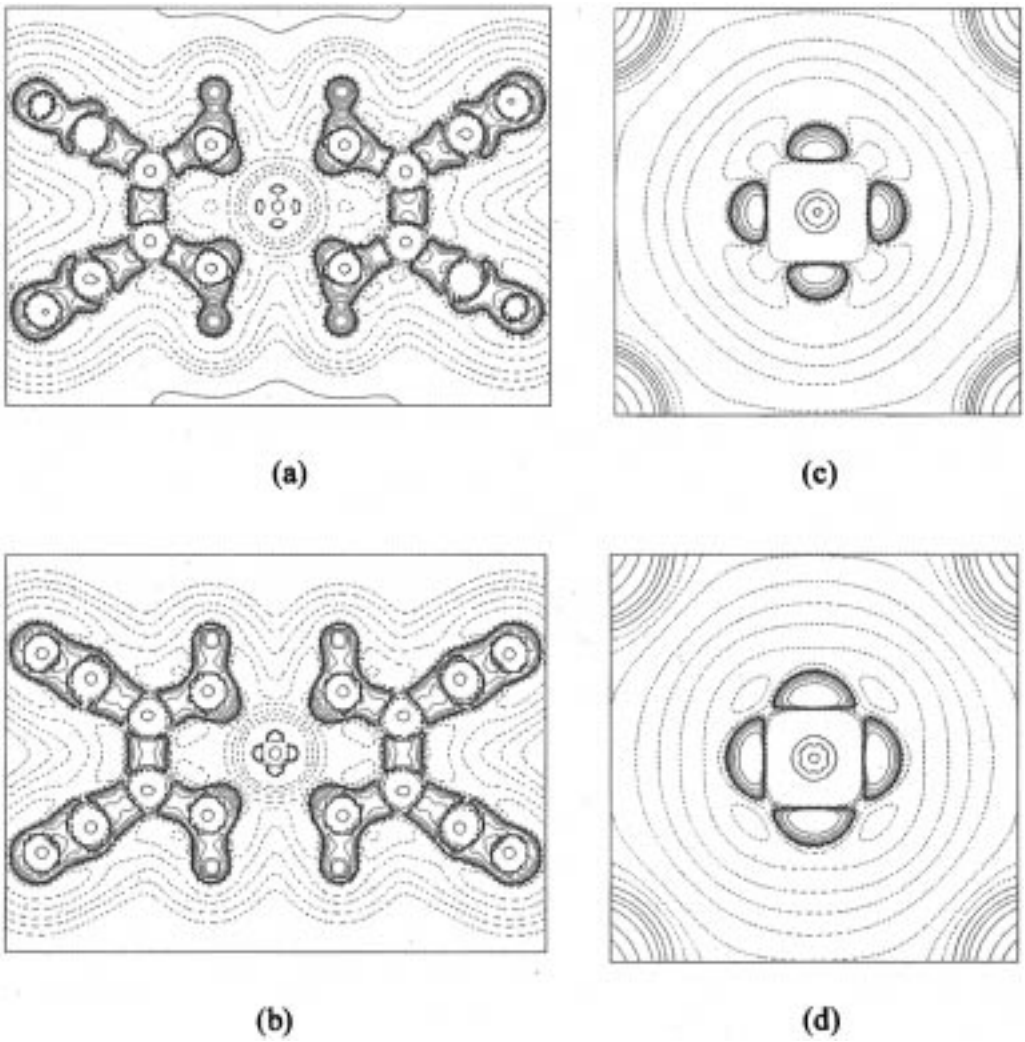

Figure 4. Negative Laplacian at the molecular plane (a, b) and the enlarged plot around Ni (c, d),where (a) and (c) are from experiment and (b) and (d) are from calculation. Contours are $(2^i \times 10^j$ eÅ^{-5}, $(i = 1, 2, 3)$, where $j = -1, 0, 1$ for (a, b) and $j = 0, 1, 2$ for (c, d). The solid red line means positive, the broken blue line negative, and the green line zero values.

N−H bond has a value of 1.6 e Å^{-3}, and Ni−N, 0.94 e Å^{-3}. The π-bond character is also indicated in the bond ellipticity, ϵ ($\lambda_1/\lambda_2 - 1$) value; for example, the N−H single bond and C5−N5 triple bond are essentially cylindrically symmetric bonds, so the ϵ value is very small (<0.05). In contrast, the ϵ values of the ring C−C and C−N bond are greater than 0.2, which strongly supports a π bond character perpendicular to the molecular plane.

Laplacian of the Electron Density

The zero isovalue envelope surface of the Laplacian, $\nabla^2\rho$, obtained from the calculation is displayed in Figure 3. This surface separates the valence shell charge concentration (VSCC $\nabla^2\rho < 0$) from the region of charge depletion ($\nabla^2\rho > 0$). This surface encompasses the VSCC of each nucleus, (3, −3) CP, and is continuous to the VSCC on the bonded atoms. The Ni−N bonds, in contrary, show little charge concentration along the bond. To further characterize the local charge concentration and the local charge depletion in the molecule, the negative Laplacian of the molecule is depicted in Figure 4. For the ring C, N atoms of the ligand, each displays three local concentrations of electron density around the nucleus; this signifies an sp^2-type of valence shell. The exocyclic C and N nuclei show two local concentrations in a linear fashion expected from a sp-hybrid valence shell. The most exciting feature of the negative Laplacian distribution is around the transition metal Ni nucleus. If one looks at the enlarged map of Ni (Figure 4b,d), it is clearly shown that the local concentrations of electron density are at the bisection of two ∠N1−Ni−N2 angles and the charge depletions are along the Ni−N directions. This is exactly in accord with the form predicted by the crystal field theory, where electron density in the valence shell is depleted in d_σ (along Ni−N) and is accumulated along the d_π direction (bisection of ∠N1−Ni−N2). Again the agreement between the experiment (Figure 4a,b) and the theory (Figure 4c,d) is satisfactory. Such a feature of the asphericity in electron density around Ni was also found in the deformation density distribution.[1]

Atom Domain

According to Bader et al.,[2] every atom, whether free or bound, is assigned to have its own unique space. The space of a bound atom is often delimited by curved surfaces because of its interaction with neighbors. This space is transferable to an atom with a similar coordination environment. The collection of atomic domains yields an atlas for the molecule. The atom domain can be identified as a zero flux surface around each atom. Such partitions projected on the molecular plane together with the total electron density and bond paths are illustrated in Figure 5 both from experiment (Figure 5a) and from MO calculation (Figure 5b). Again the comparison between experiment and theory is good with the shape and the areas of the domains are nearly superimposable on each other.

Fermi-Hole Function and Electron Delocalization

A correlation function is defined by McWeeny[7,23] to attribute the relationship between the Fermi correlation and the spatial localization of electrons. The Fermi-hole function is a distribution function for an electron of a given spin that determines the decrease in the probability of finding another electron with the same spin relative to a fixed position of the electron in question (reference electron). Thus the Fermi hole describes the region where the charge of the reference electron is spread out in space.

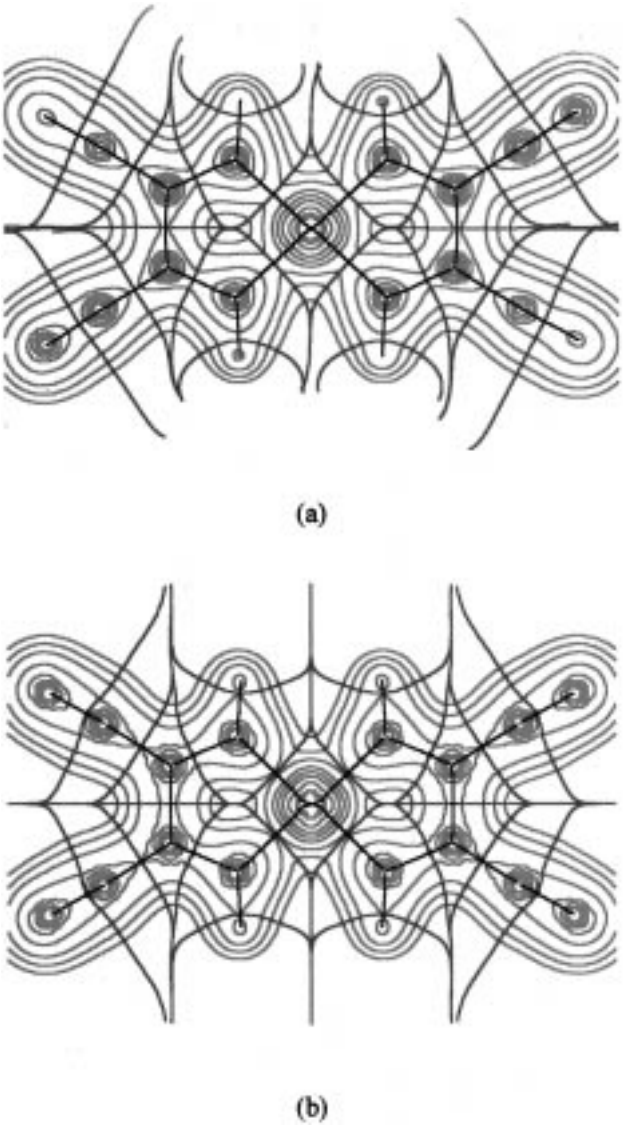

Figure 5. Total electron density (red), $\rho(\mathbf{r})$, bond path (black), and atom domain separated with green lines from (a) experiment and (b) calculation. Contours of $\rho(\mathbf{r})$ are as in Figure 4a.

This function can only be derived by MO calculation. Accordingly, the Fermi hole can provide information about the localization or delocalization of the electron density. Recently such delocalization properties of the Fermi-hole density have been utilized to quantitatively assess the delocalization of electrons in some aliphatic and aromatic compounds.[38] Here we try to use the same idea to analyze the π-delocalization of the ligand. On the basis of the bond distances of the molecule,[1] the ligand, disn, is best described as a totally π-electron delocalized monoanionic form.[39,40] Fermi-hole densities with reference electron located at 0.7 au above the molecular plane (π-density) on various atomic sites of the ligand are displayed in Figure 6a−d. Apparently π-density at the nitrilo C and N atoms (Figure 6b,d) is essentially distributed between the neighboring atoms; that is, the bond is a localized π-bond. In contrast, when the reference electron is placed on any ring C or N atom, the Fermi-hole density is spreading out to all eight ring atoms. (Figure 6a,c) This result reemphasizes the fact that the ligand is a totally π-electron delocalized monoanionic form, which is consistent with the result from earlier NBO analysis.[1] Figure 6e indicates the bond interaction between ring N and Ni at the molecular plane (σ-density); this manifests that although the Ni−N bond is largely dative indicated from the positive

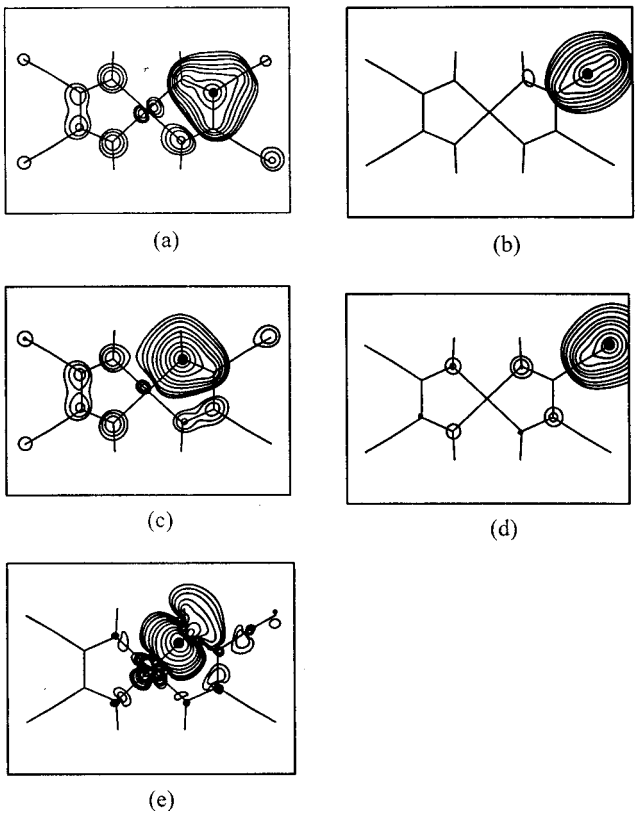

Figure 6. Fermi-hole functions at the plane of 0.7 au above the molecular plane with the reference electron (●) placed on this plane at (a) N1, (b) Cl, (c) C5, (d) N5, and (e) Fermi−hole functions at the molecular plane with reference electron situated at N1.

$\nabla^2\rho(\mathbf{r}_c)$, there is still some covalent character along this bond, again consistent with the earlier NBO results.[1]

Molecular Electrostatic Potential

MEP is often used as a tool to correlate structure and reactivity of a molecule. However it is only applied in the case where the classical Coulombic interaction is dominant, such as in protonation processes and in hydration phenomena. In general, the MEP has long been used as a reactivity index of long-range chemical interactions.[27−33,42] Many studies of MEP are based on molecular orbital calculations. It would be very useful to be able to obtain accurate values of $\rho(\mathbf{r})$ and electrostatic potential, $V(\mathbf{r})$, directly from experiment[43,44] to compare with the quantum mechanical calculation or to test the accuracy both on experiment and on theory. Here we present in Figure 7 the MEP of the molecule both from the multipole model and from the HF calculation. It is pleasing to see that the agreement between them is very good with the minimum potential of -0.1 e Å^{-1} (33.2 kcal/mol) located at the nitrilo-N atom. The intermolecular interaction cannot be addressed properly here since the electron density is calculated only for one molecule both in experiment and in theory, though the multipole coefficients are indeed affected somewhat by the crystal packing force, if there is any. For this molecular crystal, such crystal packing force is assumed to be small. However, electrostatic potential (EP) based on the calculated structure F_c model[41] can be used for understanding the intermolecular interactions such as a hydrogen bond.[10]

Conclusion

The combined experimental and molecular orbital calculated electron densities accompanied by their topological analyses are used to give a quantitative characterization of bonding. The Ni−N bond is classified as mainly a closed-shell interaction with some covalent character while all the intraligand bonds are shared interactions or covalent bonds. The π-delocalization on the ligand is clearly indicated by bond critical point properties and by the Fermi-hole function. Atom domains in the molecule are illustrated to be correlated with the atomic hybrid types in their valence shells. For all these properties, comparison is made between experiment and theory.

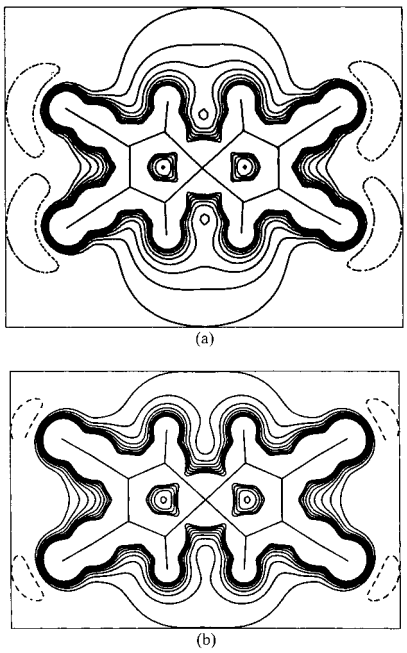

Figure 7. Molecular electrostatic potential calculated from (a) experiment and (b) calculation, where contour intervals are in 0.1 e Å^{-1} (33.2 kcal/mol) units.

Acknowledgment. Financial support of this work from National Science Council of ROC is appreciated. Thanks are due to the National Center for High Performance Computing for providing computing facilities and software packages. Special thanks to Professor R. F. W. Bader and Professor M. Souhassou for their kindly supplying a copy of the AIMPAC and PROP programs, respectively.

References and Notes

(1) Lee, C. S.; Hwang, T. S.; Wang, Y.; Peng, S. M.; Hwang, C. S. *J. Phys. Chem.* **1996**, *100*, 2934−2941.

(2) Bader, R. F. W. *Atom in Molecules-A Quantum Theory*; Clarendon Press: Oxford, U.K., 1990.

(3) Schwarz, W. H. E.; Ruedenberg, K.; Mensching, L. *J. Am. Chem. Soc.* **1989**, *111*, 6926−6933.

(4) Kunze, K. L.; Hall, M. B. *J. Am. Chem. Soc.* **1986**, *108*, 5122.

(5) Dunitz, J. D.; Seiler, P. *J. Am. Chem. Soc.* **1983**, *105*, 7056.

(6) Spasojevicdebire, A.; Dao, N. Q.; Strich, A.; Thieffry, C.; Benard, M. *Inorg. Chem.* **1990**, *29*, 4908−4915.

(7) Bader, R. F. W. *Chem. Rev.* **1991**, *91*, 893.

(8) MacDougall, P. J.; Hall, M. B.; Bader, R. F. W.; Cheeseman, J. R. *Can. J. Chem.* **1990**, *67*, 1842.

(9) Sierraalta, A.; Ruette, F. *Int. Quantum Chem.* **1996**, *60*, 1015−1026.

(10) Flensburg, C.; Larsen, S.; Stewart, R. F. *J. Phys. Chem.* **1995**, *99*, 10130−10141.

(11) Koritsanszky, T.; Buschmann, J.; Luger, P. *J. Phys. Chem.* **1996**, *100*, 10547−10553.

(12) Yufit, D. S.; Mallinson, P. R.; Muir, K. W.; Kozhushkov, S. I.; Demeijere, A. *Acta Crystallogr.* **1996**, *B52*, 668−676.

(13) Howard, S. T.; Hursthouse, M. B.; Lehmann, C. W.; Poyner, E. A. *Acta Crystallogr.* **1995**, *B51*, 328−337.

(14) Smith, G. T.; Mallinson, P. R.; Frampton, C. S.; Farrugia, L. J.; Peacock, R. D.; Howard, J. A. K. *J. Am. Chem. Soc.* **1997**, *119*, 5028−5034.
(15) Stewart, R. F. *J. Chem. Phys*. **1969**, *51*, 4569−4577.
(16) Hansen, N. K.; Coppens, P. *Acta Crystallogr*. **1978**, *A34*, 909.
(17) Hirshfeld, F. L. *Isr. J. Chem*. **1977**, *16*, 226.
(18) Silvi, B.; Savin, A. *Nature* **1994**, *371*, 683−686.
(19) Bader, R. F. W.; Johnson, S.; Tang, T.-H.; Popelier, P. L. A. *J. Phys. Chem*. **1996**, *100*, 15398−15415.
(20) Bader, R. F. W.; Gillespie, R. J.; MacDougall, P. J. *J. Am. Chem. Soc.* **1988**, *110*, 7329.
(21) Gillespie, R. J. *Can. J. Chem*. **1992**, *70*, 742.
(22) Bader, R. F. W.; Popelier, P. L. A.; Chang, C. J. *J. Mol. Struct. (THEOCHEM)* **1992**, *255*, 145.
(23) McWeeny, R. *Rev. Mod. Phys*. **1960**, *32*, 335.
(24) Bader, R. F. W.; Stephens, M. E. *Chem. Phys. Lett*. **1974**, *26*, 445.
(25) Bader, R. F. W.; Stephens, M. E. *J. Am. Chem. Soc.* **1975**, *97*, 7391.
(26) Politzer, P.; Truhlar, D. G. *Chemical Applications of Atomic and Molecular Electrostatic Potential*; Plenum Press: New York, 1981.
(27) Lin, K. J.; Cheng, M. C.; Wang, Y. *J. Phys. Chem.* **1994**, *98*, 11685−11693.
(28) Lugue, F. J.; Orozco, M.; Illas, F.; Rubio, J. *J. Am. Chem. Soc*. **1991**, *113*, 5203.
(29) Faerman, C. H.; Price, S. L. *J. Am. Chem. Soc*. **1990**, *112*, 4915.
(30) Stone, A. *J. Chem. Phys. Lett*. **1981**, *83*, 233.
(31) Stone, A. J.; Alderton, M. *Mol. Phys*. **1985**, *56*, 1047.
(32) Murray, J. S.; Lane, P.; Politzer, P. *J. Mol. Struct.(THEOCHEM)* **1990**, *209*, 163.
(33) Murray, J.; Redfern, P. C.; Lane, P.; Politzer, P. *J. Mol. Struct-.(THEOCHEM)* **1990**, *207*, 177.
(34) Wachter, A. J. H. *J. Chem. Phys.* **1907**, *52*, 1033. (b) Gianolo, L.; Pavani, R.; Clementi, E. G. *Chim. Ital*. **1978**, *108*, 181.
(35) Frisch, M. J.; Trucks, G. W.; Schlegel, H. B.; Gill, P. M. W.; Johnson, B. G.; Robb, M. A.; Cheeseman, J. R.; Keith, T. A.; Petersson, G. A.; Montgornery, J. A.; Raghavachari, K.; Al-Laham, M. A.; Zakrzewski, V. G.; Martin, R. L.; Ortiz, J. V.; Foresman, J. B.; Cioslowski, J.; Stefanov, B. B.; Nanayakkara, A.; Challacombe, M.; Gomperts, R.; Fox, D. J.; Binkley, J. S.; Defrees, D. J.; Baker, J.; Stewart, J. P.; Head-Gordon, M.; Conzalez, C.; Pople, J. A. *Gaussian 94*, revision A.1; Gaussian Inc.: Pittsburgh, PA, 1995.
(36) PROP program: A program developed by M. Souhassou, N. K. Hansen, E. Stevens, B. Craven, N. Bouhmeida, N. Ghermani, and C. Lecomte.
(37) *AIMPAC: a set of programs for the Theory of Atom in Molecules*; Bader, R. F. W., and co-workers, Eds.; McMaster University: Hamilton, Ontario, Canada.
(38) Bader, R. F. W.; Streitwieser, A.; Neuhaus, A.; Laidig, K. E.; Speers, P. *J. Am. Chem. Soc*. **1996**, *118*, 4959.
(39) Peng, S. M.; Simon, A.; Wang, Y.; Liaw, D. S. *Angew. Chem., Int. Ed. Engl*. **1985**, *24*, 210.
(40) Adams, D. M.; Dei, A.; Rheingold, A. L.; Hendrickson, D. N. *J. Am. Chem. Soc.* **1993**, *115*, 8221.
(41) Stewart, R. F. *God. Jugosl. Gent. Kristalogr*. **1982**, *17*, 1.
(42) Fan, J. M.; Wang, Y.; Ueng, C. H. *J. Phys. Chem.* **1993**, *97*, 8193−8199.
(43) Espinosa, E.; Lecomte C.; Ghermani, N. E.; Devemy, J.; Rohmer, M. M.; Benard, M.; Molins, E. *J. Am. Chem. Soc.* **1996**, *118*, 2501−2502.
(44) Su, Z. W.; Coppens, P. *Acta Crystallogr*. **1992**, *A48*, 188.